University of Ljubljana
Faculty of Mathematics and Physics

Measuring small forces with atomic force microscope

Author: Matjaž Humar
Adviser: Dr. Igor Muševič

April 17, 2006

Abstract

Atomic Force Microscope (AFM) is a versatile tool for the characterization of the nanostructures. It is useful in visualizing surfaces as also in measuring small forces down to 10^{-12} N. With the force curves we can measure mechanical proprieties of the samples. Different imaging modes enable the mapping of various characteristics of the sample (height, friction, electric potential, magnetic field, etc.).

With the three point bending method I determined mechanical proprieties of titania-derived nanoribbons. The measured Young's modulus of nanoribbons is 260 GPa. Because of good elastic properties of titania-derived nanoribbons, they can be mixed with polymers, thus reinforcing the composite materials.

Contents

1 FUNDAMENTALS OF ATOMIC FORCE MICROSCOPY

1.1 History of Atomic force Microscopy

Scanning Probe Microscopy (SPM) is a family of related techniques that provide information about atomic scale structure and processes. The first of these to be developed was the Scanning Tunneling Microscope (STM) by Gerd Binning and Heinrich Rohrer at IBM Zurich in 1981 [1, 2]. In 1986 Binnig, Calvin Quate and Christopher Gerber invented another scanning probe instrument called the Atomic Force Microscope (AFM) [3]. These powerful techniques and others have been rapidly adopted by the scientific community and applied in numerous fields ranging from biology to materials science. The number of publications and patents in the SPM field has increased exponentially over the last twenty years. In 1984 there were 16 publications utilizing scanning probe microscopy, whereas in 2003 there were over 10,000. Since the conception of the STM and the AFM, many other scanning probe techniques have been devised that have helped scientists understand chemical and physical phenomena that occur on the nano-scale.

1.2 Fundamentals of Atomic Force Microscopy

AFM operates in the following manner: a cantilever beam with a sharp tip on the end is brought into close proximity with the surface of a sample. The sample is rastered below the cantilever. Sample topography and forces exerted between the tip and the sample cause upward or downward deflections of the cantilever. These deflections are stored in a computer and represent image of a surface.

Figure 1: Digital Instruments AFM. [4]

1.3 Parts of an Atomic Force Microscope

1.3.1 Detectors

Movement of the cantilever is typically tracked by illuminating the reflective back-side of the cantilever with a laser and monitoring the movement of the reflected spot on a position-sensitive detector (Figure 2a). The voltage output from the detector is proportional to the position of the movement of the laser spot on the face of the detector. The quadrant-photodiode is capable of measuring vertical cantilever deflection as well as cantilever torsion. Integration of a detector onto

the cantilever (i.e. strain gauge) has also been accomplished using the piezoresistive properties of doped silicon (Figure 2b). This eliminates the laser and the position sensitive detector. This approach is beneficial for imaging samples that are light sensitive or when the cantilever is immersed in a nontransparent liquid.

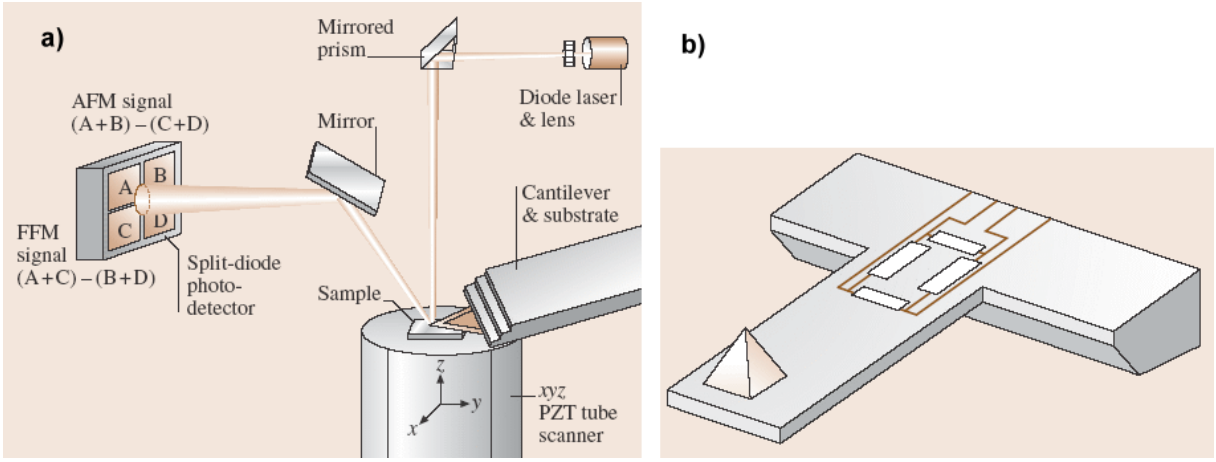

Figure 2: Cantilever movement is typically tracked by (a) monitoring the movement of the reflected spot on a position-sensitive detector or (b) integration of a detector onto the cantilever. [5]

1.3.2 Vibration Isolation

The entire microscope is mounted on a vibration isolation apparatus. Vibration isolation units can range from simple units such as a concrete block hanging from bungee-cords to vibration isolation tables that have pneumatically suspended tabletops. If external noise is not controlled or reduced, visualizing the atomic-scale features is impossible.

1.3.3 Piezoelectric Scanners

Piezoelectric tubular scanners are the most commonly used. They have high mechanical resonance frequency, enabling high scan rates. Application of precisely controlled voltages to a piezoelectric produce extremely precise movements. Piezoelectric scanners exhibit both linear and nonlinear responses to an applied voltage. As a result, careful scanner calibration is required. The sample can be mounted directly onto the scanner and rastered underneath the cantilever tip, or the cantilever can be mounted to a scanner tube and rastered over a sample fixed below it. Samples for analysis are mounted onto a specimen disk that can be magnetically held onto the piezoelectric scanner.

1.3.4 Cantilevers

Cantilevers are commercially produced from silicon and silicon nitride using microfabrication processes similar to those employed in integrated circuit manufacture. Cantilevers are often coated with metal on the topside to enhance laser reflection. Important cantilever specifications are their dimensions,

flexibility, and resonance characteristics (resonance frequency and quality factor). Resonance frequencies can be calculated by solving differential equation

$$u^{IV}(x,t) = -\frac{m_0}{EJl}\ddot{u}(x,t). \tag{1}$$

For first three resonant frequencies we get

$$\omega_i = \left(\frac{w_i}{l}\right)^2 \left(\frac{EJl}{m_0}\right)^{\frac{1}{2}} \tag{2}$$

where

$$w_1 = 1.875, \qquad w_2 = 4.694, \qquad w_3 = 7.855, \qquad \ldots \tag{3}$$

The fundamental resonance frequency of the cantilever should be high in order to avoid interference from building vibrations and acoustic noise (1 Hz - 100 Hz). Typical spring constants for AFM cantilevers range from 0.01 N/m to 100 N/m, enabling a force sensitivity down to 10^{-12} N. The limit in force sensitivity is dependent on thermal, electrical and optical noise. Thermal fluctuations of the cantilever are equal to

$$\Delta E = \frac{1}{2}k\langle \Delta z^2 \rangle = \frac{1}{2}k_B T \tag{4}$$

$$\Delta z = \sqrt{\frac{k_B T}{k}}. \tag{5}$$

Using $F = kz$ we can calculate the uncertainty of the measured force which is 0.1 nN for $k = 1$N/m at room temperature. The equivalent Δz is 0.1 nm. Therefore thermal noise from the cantilever can be minimized by using cantilevers with larger spring constant. A shorter length cantilever also provides greater angular displacement of the laser resulting in better resolution. Cantilever tip shape and dimensions are critical to the quality of the AFM image. The overall tip geometry is often square pyramidal resulting from an etching process (Figure 3b).

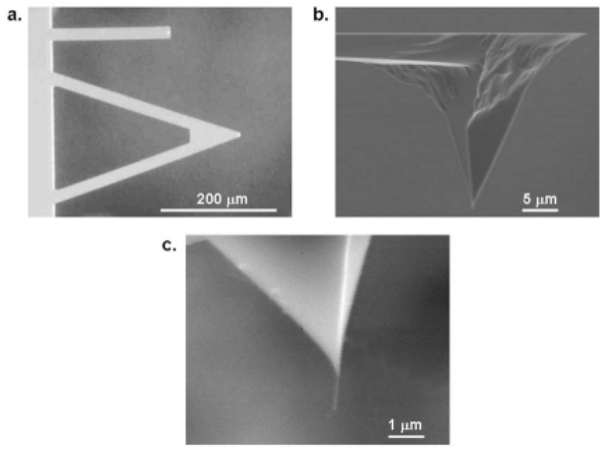

Figure 3: (a) Cantilevers of different shapes and spring constants on a single silicone nitride chip, (b) sharpened tip at the ent of the cantilever, (c) a carbon nanotube mounted on the tip apex. [6]

Tip sharpness, or the radius of curvature at the apex, is one of the key elements in achieving high-resolution images (Figure 4). Both tip contamination or general wear (mechanical rounding)

can drastically reduce image resolution. Recently, carbon nanotubes have become popular tips because of their high aspect ratio, small radius of curvature, and durability (Figure 3c). Tips are often functionalized in order to study tip to sample interactions or to conduct chemically sensitive measurements.

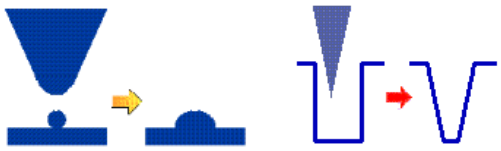

Figure 4: The final picture from the AFM is a convolution between the shape of the tip and the shape of the sample. [6]

1.4 Imaging Modes

The atomic force microscope can be operated in several modes: contact, torsional, force modulation, intermittent contact, non-contact and force volume. Each imaging mode can provide different information regarding the chemical and physical nature of a surface. Several other imaging modes have been developed over the years but the following modes of operation are still the most widely used.

1.4.1 Contact Mode

In this mode, the probe tip is maintained in contact with the sample surface. The image can be acquired under four different imaging methods: deflection, height, friction, and force modulation. In the deflection method, the image is a map of cantilever bending as a function of position and is acquired under variable vertical loading forces. To image under constant applied force, the height method uses a closed-loop feedback system to raise or lower the sample (or tip) to maintain a nearly fixed cantilever deflection.

1.4.2 Force Curves

Force curves are used to correlate vertical movement of the scanner with cantilever deflection. An "ideal" force curve is shown in Figure 5a. Force curves are obtained by disabling the scanner movement in the x and y directions and extending and retracting the scanner in the z-direction. As the tip approaches the sample, no cantilever bending is observed until the gap between the tip and the sample is extremely small (typically < 1 nm). At this point, attractive van der Waals interactions between the tip and the substrate will pull the cantilever downward. Once in contact, raising the sample produces an upward bend in the cantilever. On the downward movement of the scanner, the cantilever gradually returns to its original position. Eventually the scanner is retracted far enough away from the cantilever until the tip and the surface are separated. In the presence of attractive or adhesive forces, downward deflection of the cantilever may be observed. When the restoring force of the cantilever exceeds these forces, the tip is released from the substrate

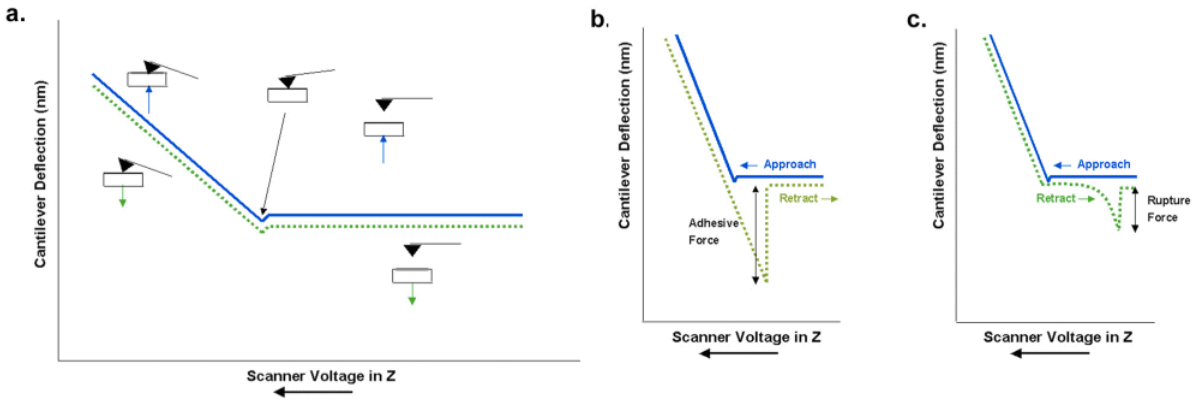

Figure 5: (a) Force curve in vacuum, (b) force curve in air or when other adhesive forces exist, (c) when a molecule gets attached to the tip and than suddenly breaks off. [7]

surface and the cantilever returns to its original position (Figure 5b). The force is computed by multiplying the total vertical deflection of the cantilever times its spring constant. Force curves enable calibration of the cantilever deflection and commensurate movement of the laser spot on the PSD. This is accomplished by fitting a line to the portion of the force curve where the scanner is pushing up on the cantilever beam.

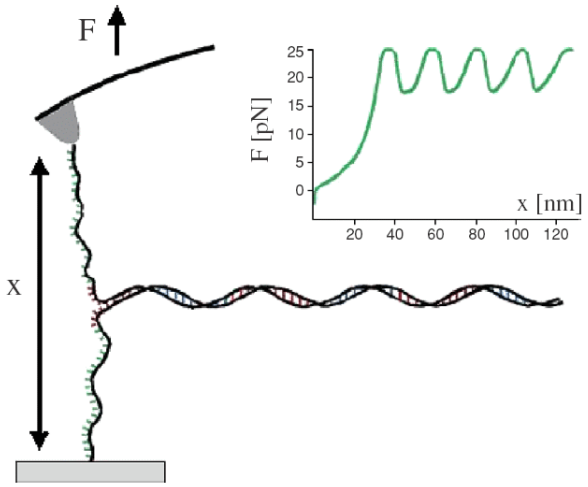

Figure 6: Example of AFM force measurement. DNA molecule is torn apart, with clearly visible single base pairs breaking apart. [6]

1.4.3 Friction Force Microscopy

Friction force microscopy measures the local variations of friction that may exist between the cantilever tip and the substrate. Lateral forces on the tip cause torsional bending (twisting) of the cantilever that is detected by horizontal movement of the laser spot on the quadrant photodiode (Figure 7).

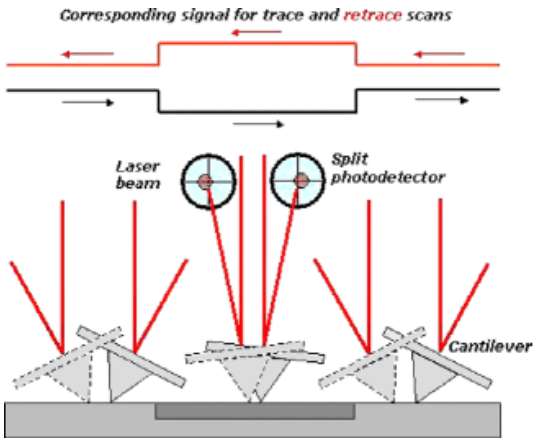

Figure 7: Friction between the tip and the surface makes the cantilever to torsional deform. [7]

1.4.4 Intermittent Contact Mode

Intermittent contact or Tapping mode oscillates the cantilever at its resonance frequency or one of the higher vibrational modes. The frequencies are typically around 100 kHz. To operate in the intermittent contact mode, the cantilever chip is mounted into a holder that mechanically oscillates the entire cantilever chip. Surface topology is measured with the height method, while maintaining constant dampening of cantilever oscillation rather than cantilever measuring beam deflection, as is done in contact mode. Cantilever oscillation amplitude dampening is maintained at a fixed value using a closed-loop feedback system to raise or lower the sample. The major advantages of intermittent contact mode imaging are reduced vertical loads, lateral forces, and adhesive interactions between the tip and the substrate. This mode enables imaging of soft samples or molecules that are not strongly attached to the surface.

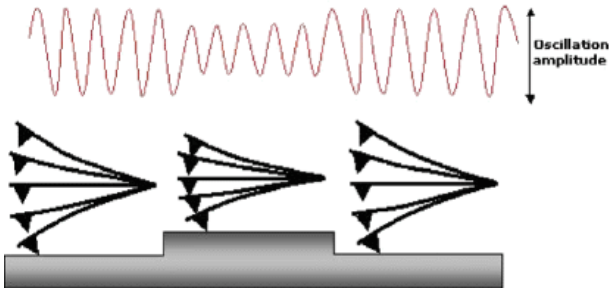

Figure 8: Principle of tapping mode. [6]

1.4.5 Phase Imaging

Phase imaging is an extension of intermittent contact mode that enables measurement of surface properties such as adhesion, friction, and elasticity. Phase imaging detects the phase shift of the cantilever oscillation relative to the oscillation driving signal. Phase shifts above 90° are due to attractive interactions, whereas phase shifts below 90° are due to repulsive interactions. Phase

imaging has become the workhorse tool for analyzing the elasticity of composite materials. For topologically homogeneous surfaces, more elastic domains are readily distinguished from less elastic regions in the phase image.

1.4.6 Noncontact Mode

Noncontact mode imaging relies on longer-range molecular forces to obtain surface topology. The cantilever is oscillated at its resonance frequency, as in the tapping mode. The surface topography is measured by monitoring the shifts in cantilever resonant frequency. The new cantilever's resonance frequency is calculated using Eq. (1) with force gradient added. We get

$$f = 9.57\sqrt{\frac{1}{M}\left(k + \frac{dF_z}{dz}\right)} \tag{6}$$

where k is the spring constant, M the mass of the cantilever and F the force between the tip and the surface.

Two types of non contact mode are:

Electric force microscopy (EFM) is based upon measuring Coulomb forces between electrical charged microscope tip and the sample. In this way the tip is not touching the surface, making possible to image very soft samples and even fluid droplets. It is also possible to measure electrostatic potentials of single molecules.

Magnetic force microscopy (MFM) In the magnetic force microscopy dipole-dipole interactions between the ferromagnetic tip and the sample are measured (Figure 9).

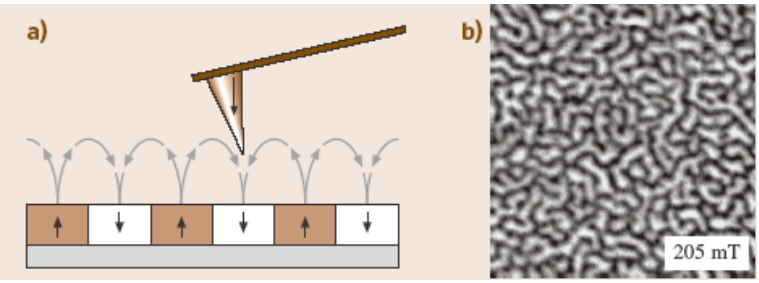

Figure 9: (a) Principle of MFM operation (b) Field-dependent domain structure of a ferromagnetic thin film. [5]

1.4.7 Force Volume Imaging

Force volume imaging is an extension of contact mode AFM. A sample is translated underneath the cantilever in the x, y and z direction via the piezo-scanner. As the sample moves in x and y, a topographical image of the underlying sample is generated. For every pixel in the topographical

image, a corresponding z-movement is executed (extension and retraction of the scanner). The z-movement of the sample yields a force curve. These force curves can provide data about the adhesion forces and local mechanical proprieties of a large area of a sample.

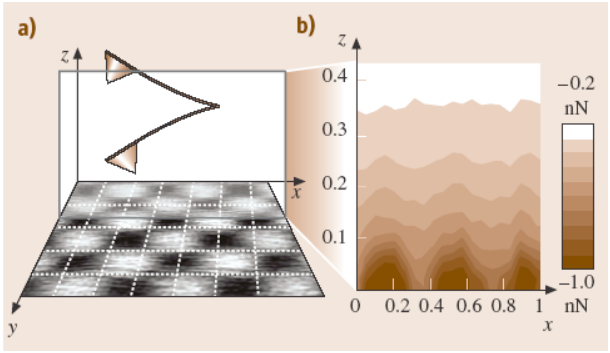

Figure 10: (a) Principle of the 3-D force filed spectroscopy (b) A 2-D cut through the 3-D force field $F_{ts}(x, y, z)$. [5]

2 EXPERIMENTAL WORK

2.1 Introduction

Nanomaterials are becoming industrially interesting mainly because of their potential multifunctional operation. For instance, it is desirable that these materials combine special electronic, chemical and/or mechanical properties. Carbon nanotubes, for instance, are typical examples of such materials displaying mesoscopic transport properties, while having astonishing mechanical properties [9]. In recent years it has also been demonstrated that nanotubes can be prepared from different inorganic materials, such as MoS_2 [10][11][12], boron nitride [13] or titanium dioxide [14][15]. Titania is a well-known industrial catalytic and photo-catalytic material [16]. It can be used in solar cells, antibacterial coatings and for the removal of pollutant gases, such as NO_x [17]. The titania nanostructures are usually mixed with a polymer matrix to form a composite. If this nanostructures have good mechanical properties, they can improve mechanical stability of the composite. I have therefore decided to investigate the Young's modulus of titania-based nanotubes and nanoribbons, using the same method as developed for carbon nanotubes [9].

2.2 Experimental

Titania based nanotubes and nanoribbons were synthesized by using standard hydrothermal method [17], which consists of mixing titania anatase powder with sodium hydroxide and heating for several hours. Depending on the temperature, either nanotubes or nanoribbons were grown (Figure 11). With contact AFM and TEM imaging we measured typical lengths and diameters of these structures.

The nanotubes are hollow with outer diameters of 8-11 nm, inner diameters between 4-7 nm, and lengths of several hundred nanometers. The nanotubes (Figure 11a) are scrolls as revealed by

the unequal number of walls on the two tube sides, and occasional end-on views within the images. However, when the material was treated at higher temperatures, facetted nanoribbons with typical widths of about 40 nm and lengths from several hundred nanometers to several micrometers formed (Figure 11b). Both nanotubes and nanoribbons have similar structure, which is closely related to the family of the layered titanate $(Na,H)_2Ti_nO_{2n+1}$ materials [18][19].

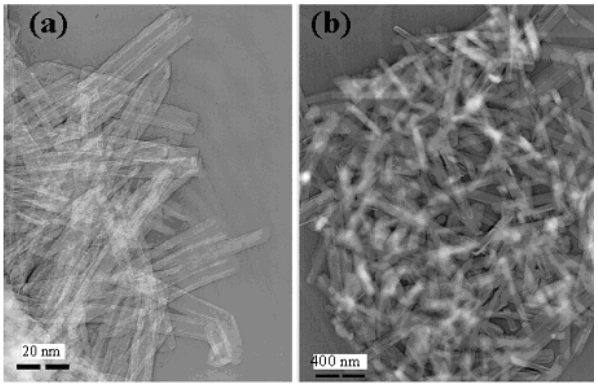

Figure 11: (a) TEM image of titania-based nanotubes and (b) of nanoribbons. [17]

In order to measure Young's modulus I used three point bending method [9][20]. As a substrate I used CR-39 polymer, previously bombarded with fast ions and then etched. In this way I achieved a smooth surface with holes with diameters around 1 μm. Nanoribbons were ultrasonically dispersed in methanol. The dispersion was dripped to the substrate and methanol was left to evaporate. In this way the nanoribbons were randomly deposited to the substrate (Figure 12).

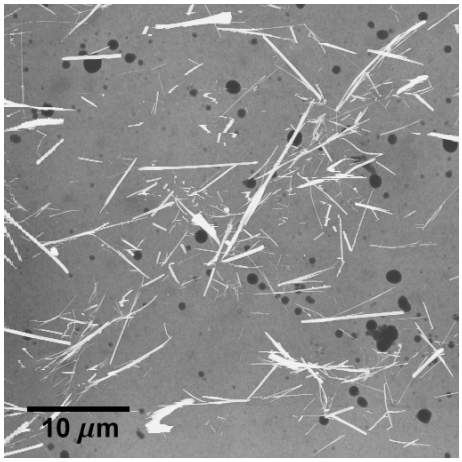

Figure 12: Nanoribbons deposited to the CR-39 substrate with holes.

Some nanoribbons laid over the holes with a very good contact with the substrate on both ends (Figure 16). With the AFM tip I applied a load at the middle of the suspended nanoribbon and measured the deflection (Figure 13). The deflection was also measured on the part of the nanoribbon that was on the flat surface next to the hole (point B). This deflection was subtracted from the deflection measured over the hole (point C). In this way I compensated the penetration of the AFM tip into the nanoribbon and the deflection of the substrate itself. The applied force

to the nanoribbon was not bigger than 200 nN. After the deflection was measured, I checked if any permanent damage was made to the nanoribbon. All the measurements were performed with Digital Instruments IIIa atomic force microscope and silicone cantilevers with spring constant of 0.9 Nm^{-1}.

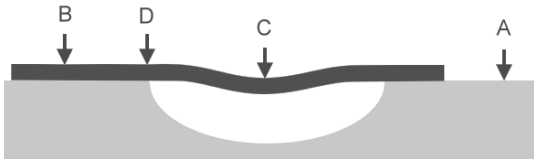

Figure 13: Points where the deflection as a function of load was measured. The deflection at B was subtracted from the deflection at C in order to compensate penetration of the tip into the nanoribbon and the deflection of the substrate. I used two extra measurement points (D and A) for control reasons.

2.3 Theoretical model

The nanoribbon was treated as a homogenous beam with rectangular profile. In order to calculate the deflection u of the beam, we must solve

$$u'''(x) = -\frac{F(x)}{EJ} \tag{7}$$

where F is the force and J is the second moment of the beam. Because of strong interaction between the nanoribbon and the substrate, I assumed that the slope of the nanoribbon at the hole edge was always zero (Figure 14). In this case the deflection $\delta = u(L/2)$ of the suspended objects is related to the Young's modulus through the relation

$$\delta = \frac{FL^3}{192EJ} \tag{8}$$

$$J = \frac{ab^3}{12} \tag{9}$$

where F is the applied load, L is the suspended length, E is the Young's modulus, a is the width and b is the height of the nanoribbon.

I have measured deflection of the cantilever versus vertical position of the sample. In this way we get linear dependence. The relation between slopes and the spring constants of the surface is described by

$$\frac{k_1}{k_2} = \frac{s_1}{s_2} - 1 \tag{10}$$

where s_1 is the slope on hard surface, s_2 is the slope on the nanoribbon over the hole, k_1 is the spring constant of the cantilever and k_2 is the spring constant for the nanoribbon (Figure 15). The whole formula for the calculation of the Young's modulus is therefore

$$E = \frac{L^3}{192J}\frac{k_1}{\frac{s_1}{s_2} - 1} \tag{11}$$

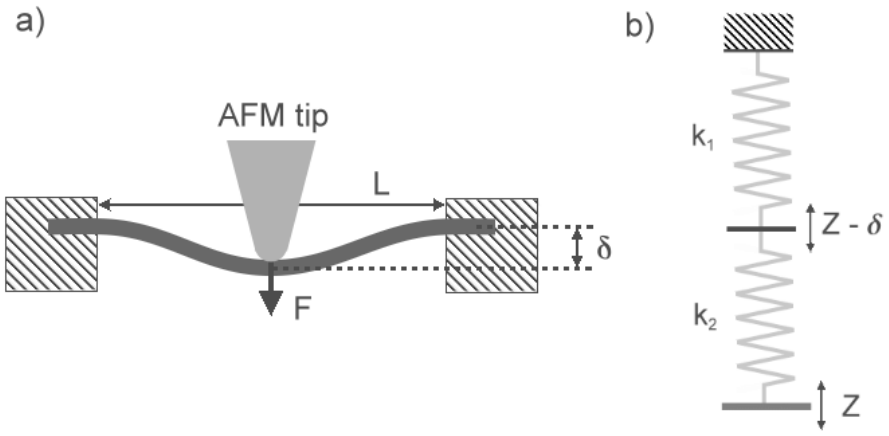

Figure 14: Configuration of the experiment.

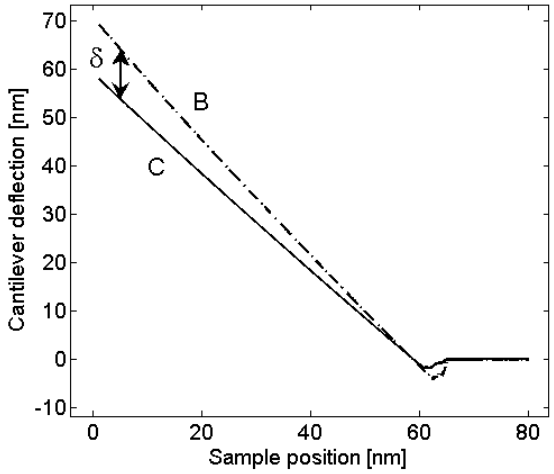

Figure 15: Example of a force curves measured in points C and B. The force curve C has the slope s_2 and the force curve B has the slope s_2.

2.4 Results and discussion

Deflection was measured on seven titania-based nanoribbons and the Young's modulus was calculated using (11). The results are summarized in Table 1.

No.	L[nm]	b[nm]	a[nm]	E[GPa]
1	755	28.0	75	101 ± 53
2	565	27.1	30	281 ± 155
3	695	33.5	67	478 ± 244
4	489	27.7	54	189 ± 102
5	292	46.4	76	140 ± 67
6	570	29.0	54	469 ± 253
7	528	28.5	49	159 ± 78

Table 1: Structural properties and bending modulus of titania-derived nanoribbons.

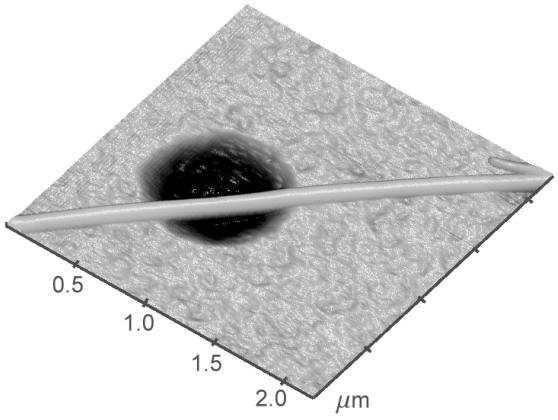

Figure 16: A typical example of a nanoribbon suspended over a hole (nanoribbon No.1 see Table 1): $L = 755$ nm ± 20 nm, $a = 28.0$ nm ± 1.1 nm, $a = 75$ nm ± 4 nm and calculated $E = 101$ GPa ± 53 GPa.

The errors of Young's modulus are rather large. Errors derive from: (i) the uncertainty in the length, width and height of the nanoribbons as I found in most cases that width and height slightly varies over the ribbon (13%)[1]; (ii) the fact that I used CR-39 substrate in a way helped us to work on a very flat well defined surface (RMS 1.5 nm), but introduced uncertainty in the elasticity of the measurements system (16%)[1]; (iii) errors in measuring the deflection of the cantilever and nonlinearities in the nanoribbon deflection (5%)[1]; (vi) and finally the uncertainty in the spring constant of the cantilever (10%)[1]. The mean Young's modulus of titania-based nanoribbons is $E =$ 260 GPa ± 55 GPa. I first note that the obtained E is similar compared to the Young's modulus of the bulk crystalline TiO_2 phase, which is about 280 GPa. However, the Young's modulus is larger than for electrospun anatase TiO_2 nanofibers [20], which is 76 GPa. One can also notice a general

[1]Errors that contribute to the final error.

trend of the decrease of the measured effective Young's modulus with increasing diameter of the nanoribbons (Figure 17).

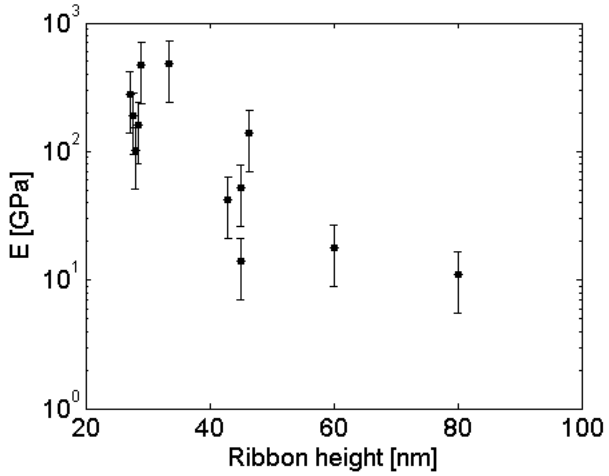

Figure 17: Young's modulus versus height of titania-based nanoribbons.

I stress that the same type of behaviour has been observed also in ropes of carbon nanotubes [9]. In the case of carbon nanotubes a shear deformations were responsible for the reduction of effective E with increasing rope diameter. It is very likely that very similar situation occurs also in our case and that the true Young's modulus of our nanoribbons may be much higher. Unfortunately I was not able to reduce the dimensions of the nanoribbons much below 30 nm to check on this. All the nanoribbons thinner than 30 nm laying over the hole, were bent into the hole as a consequence of the van der Waals force and the capillary forces in the process of methanol evaporation (Figure 18a). I also tried to determine the Young's modulus of nanotubes, but I encountered the same problem as with thin nanoribbons (Figure 18b).

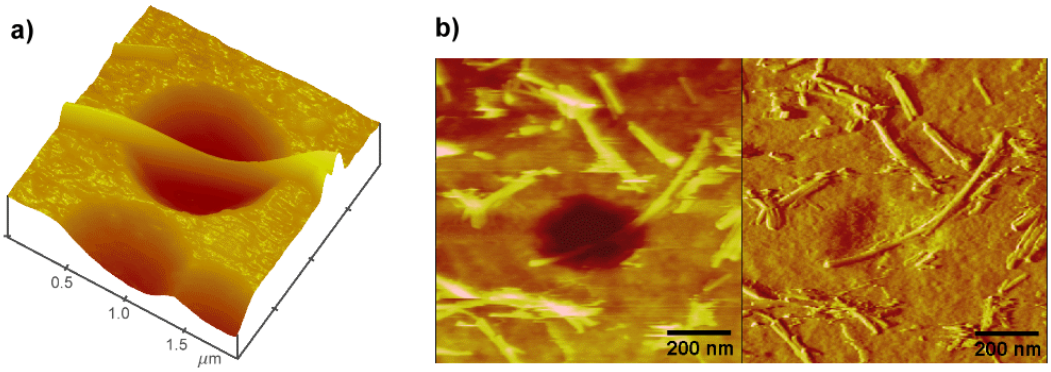

Figure 18: (a) A thin nanoribbon bent into the hole. (b) Self bending of all titania based nanotubes, made the measurement of the Young's modulus impossible.

2.5 Conclusion

I determined the mechanical properties of titania-based nanoribbons using AFM Force Spectroscopy mode of operation. The average bending modulus is 260 GPa. Present results demonstrate good elastic properties of titania-derived nanoribbons. Mixing them with polymers may thus significantly reinforce the composite materials.

2.6 Acknowledgments

I thank to D. Arčon, P. Umek, M. Škarabot, I. Muševič and G. Bregar for the help in my experimental work.

References

[1] G Binnig, H Rohrer, C Gerber, E Weibel: *Tunneling through a controllable vacuum gap. Applied Physics Letters* 1982: **40**; 178-80.

[2] G Binnig, H Rohrer: *In Touch with Atoms. Review of Modern Physics* 1999: **71**; 324-30.

[3] G Binnig, CF Quate, C Gerber: *Atomic Force Microscope. Physical Review Letters* 1986: **56**; 930-34.

[4] Digital instruments home page, *http://www.di.com.*

[5] Bhushan: *Handbook of Nanotechnology*, Springer, 2004.

[6] Andrea Alessandrini and Paolo Facci: AFM: A versatile tool in biophysics, *Meas. Sci. Technol.* **16** (2005) R65-R92.

[7] Mark Andrew Poggi: *Interfacial and Mechanical Properties of Carbon Nanotubes: A Force Spectroscopy Study*, A Dissertation, Georgia Institute of Technology, September 2004.

[8] A. Borštnik, R. Podgornik, M. Vencelj: *Rešene naloge iz mehanike kontinuov*, DMFA, 2001.

[9] J.-P. Salvetat, G.A. D. Briggs, J.-M. Bonard, R.R. Bacsa, A. J. Kulik, T. Stöckli, N.A. Burnham, and L. Forro, *Phys. Rev. Lett.* **82**, 944 (1999).

[10] M. Remškar, A. Mrzel, Z. Škraba, A. Jesih, M. Čeh, J. Demšar, P.Stadelmann, F. Levy, D. Mihailovic, *Science* **292**, (2001) 479.

[11] D. Arčon, A. Zorko, P. Cevc, A. Mrzel, M. Remškar, R. Dominko, M. Gaberšček, and D. Mihailovič, *Phys. Rev.* **B67**, 125423 (2003).

[12] R. Dominko, D. Arčon, A. Mrzel, A. Zorko, P. Cevc, P. Venturini, M. Gaberšček, M. Remškar, and D. Mihailovič, *Adv. Mater.* **14**, 1531 (2002).

[13] N.G. Chopra, R.L. Luyken, K. Cherrey, V.H. Crespi, M.L. Cohen, S.G. Louie, and A. Zettl, *Science* **269**, 966 (1995).

[14] T. Kasuga, M. Hiramatsu, A. Hoson, T. Sekino, K. Niihara, *Langmuir* **14**, 3160 (1998).

[15] T. Kasuga, M. Hiramatsu, A. Hoson, T. Sekino, K. Niihara, *Adv. Mater.* **11**, 1307 (1999).

[16] Miyauchi, M.; Nakajima, A.; Fujishima, A.; Hashimoto, K.; Watanabe, T.; *Chem. Mater.* **12**, 3 (2000).

[17] P. Umek, P. Cevc, A. Jesih, A. Glotter, C.P. Ewels, D. Arčon, submitted for a publication.

[18] A. Gloter, C. Ewels, P. Umek, D. Arčon and C. Colliex, submitted to *Phys. Rev. B.*

[19] J. Yang; Z. Jin, X. Wang, W. Li, J. Zhang, S. Zhang, X. Guo, and Z. Zhang, *Dalton. Trans.* 3898 (2003).

[20] Sung-Hwan Leea, Cagri Tekmenb and Wolfgang M. Sigmund, *Mater. Sci. and Eng.* **398**, 77-81 (2005).